THE JOURNAL OF PHYSICAL CHEMISTRY A

Subscriber access provided by University of East Anglia Library

A: Spectroscopy, Molecular Structure, and Quantum Chemistry

Spectral Filtering as a Tool for Two-Dimensional Spectroscopy: A Theoretical Model

Dale Green, Franco Valduga de Almeida Camargo, Ismael A. Heisler, Arend G Dijkstra, and Garth A. Jones

J. Phys. Chem. A, **Just Accepted Manuscript** • DOI: 10.1021/acs.jpca.8b03339 • Publication Date (Web): 09 Jul 2018

Spectral Filtering as a Tool for Two-Dimensional Spectroscopy: A Theoretical Model

Dale Green,[†] Franco V. A. Camargo[a],[†,¶] Ismael A. Heisler[b],[†] Arend G. Dijkstra,[‡] and Garth A. Jones[*,†]

†*School of Chemistry, University of East Anglia, Norwich Research Park, Norwich, NR4 7TJ, UK*

‡*School of Chemistry, University of Leeds, Leeds, LS2 9JT, UK*

¶*CAPES Foundation, Ministry of Education of Brazil, Brasilia DF 70040-202, Brazil*

E-mail: garth.jones@uea.ac.uk

[a] Current address: IFN-CNR, Dipartimento di Fisica, Politecnico di Milano, Piazza L. da Vinci 32, 20133 Milano, Italy

[b] Current address: Departamento de Fisica, Universidade Federal do Parana, Caixa Postal 19044, 81531-990 Curitiba, Parana, Brazil

Abstract

Two-dimensional optical spectroscopy is a powerful technique for the probing of coherent quantum superpositions. Recently, the finite width of the laser spectrum has been employed to selectively tune experiments for the study of particular coherences. This involves the exclusion of certain transition frequencies, which results in the elimination of specific Liouville pathways. The rigorous analysis of such experiments requires the use of ever more sophisticated theoretical models for the optical spectroscopy of electronic and vibronic systems. Here we develop a non-impulsive and non-Markovian model which combines an explicit definition of the laser spectrum, via the equation of motion-phase matching approach (EOM-PMA), with the hierarchical equations of motion (HEOM). This theoretical framework is capable of simulating the 2D spectroscopy of vibronic systems with low frequency modes, coupled to environments of intermediate and slower timescales. In order to demonstrate the spectral filtering of vibronic coherences, we examine the elimination of lower energy peaks from the 2D spectra of a zinc porphyrin monomer on blue-shifting the laser spectrum. The filtering of Liouville pathways is revealed through the disappearance of peaks from the amplitude spectra for a coupled vibrational mode.

Introduction

The proliferation of two-dimensional optical spectroscopy (2DOS) has revolutionised research into the structure and dynamics of chemical systems.[1–3] The detection of coherent quantum superpositions can identify electronic couplings and the existence of excitonic states, as well as vibronic couplings and the motions of nuclear wavepackets on a potential energy surface.[4,5] The study of such *coherences* requires the use of ultrafast spectroscopic techniques, where 2DOS provides a means of differentiating individual coherence pathways.[6] These coherences have been utilized for the investigation of energy transfer in photosynthetic light harvesting complexes,[7–17] as well as the determination of the excitonic structure of quantum dots.[18–21] Organic dye molecules and macrocycles such as cyanines,[22–24] and porphyrins,[25,26] as well as chromophores such as chlorophyll,[27–29] have been extensively studied to explore the origins of these coherences in biological complexes. Homodimers and larger aggregates are used as analogues of the multichromophoric structures.[30–36] 2DOS has also found application to studies of photochemistry and reaction dynamics.[37–42]

2DOS is a powerful technique for exploring vibronic processes, however, it is often difficult to distinguish specific spectral features from the wealth of dynamical data produced by each experiment.[43] It has been demonstrated recently that *spectral filtering* - a technique that involves focusing the laser spectrum over a specific excitation window - can be used to distinguish electronic from vibrational coherences. Camargo et al have shown experimentally that selective removal of peaks from the amplitude spectra can be achieved upon blue-shifting the laser spectrum, thereby eliminating Liouville pathways associated with lower energy transitions and allowing clearer analysis of the remaining coherences.[26] This kind of analysis has been performed recently to highlight the role of ground state vibronic wavepackets in the Fenna-Matthews-Olson complex.[44]

In this work, we describe the development of a theoretical model which reproduces the experimental 2DOS spectra of the 5,15-bisalkynyl zinc porphyrin monomer used by Camargo et al. In order to achieve this, the model requires an explicit description of the finite

laser pulses, beyond the impulsive limit, for which we adopt the equation of motion-phase matching approach (EOM-PMA).[45,46] We solve the temporal evolution using the hierarchical equations of motion (HEOM), which allows a non-Markovian description of the system-bath correlation function.[47–49] This enables the simulations to realistically model the strongly coupled, overdamped low frequency intramolecular vibrations of the zinc porphyrin monomer, accounting for ensemble effects such as inhomogeneous broadening within the evolution of the HEOM.

By combining the EOM-PMA and HEOM quantum dynamical methods, we present a rigorous model capable of performing the accurate evolution of an open quantum system on interaction with a sequence of laser pulses. The combination of these methods to investigate the effects of finite pulse widths by Leng et al highlights the potential of this model.[50] As the HEOM allows for any strength system-bath coupling and the EOM-PMA accounts for all time-ordering effects, our model is only restricted to the weak-field and dipole approximations in the system-field interaction.[51–53] An explicit definition of the coupled phonon environment within the HEOM enables the incorporation of dissipative effects, such as intramolecular vibrational relaxation (IVR) and fluorescence, as well as dephasing.

In this study, the model is applied to the Q_x band of the zinc porphyrin monomer, associated with the transition between the ground and first excited singlet states. The maximum of the fundamental transition occurs at $15\,650\,\mathrm{cm}^{-1}$, with a vibronic shoulder on the blue side, identifying coupling to a vibrational mode of $375\,\mathrm{cm}^{-1}$.[26] The amplitude spectra of the coupled vibrational mode are calculated using two different laser spectra, one which is centred at the fundamental transition frequency, and another which has been blue-shifted such that the lower energy transition, equivalent to the first hot band, is covered by significantly less intensity. We begin with an overview of key features of the model, greater detail of all sections is available in the SI.

Theoretical Methods

The vibronic Hamiltonian, eq 1, has an electronic ground state, $|g\rangle$, (S_0) and a single excited state, $|e\rangle$, (S_1) that lies $\hbar\omega_{eg}^0$ above the ground state equilibrium position,[1]

$$H_S = |g\rangle h_g \langle g| + |e\rangle h_e \langle e| \tag{1}$$

We assume all nuclear modes are harmonic, giving rise to vibronic terms in the Hamiltonian of,[54]

$$h_g = \hbar\omega_0 \left(b^\dagger b + \tfrac{1}{2}\right) \tag{2}$$

$$h_e = \hbar(\omega_{eg}^0 + \lambda) + \hbar\omega_0 \left(b^\dagger b - \frac{\Delta}{\sqrt{2}}(b + b^\dagger) + \tfrac{1}{2}\right) \tag{3}$$

where $b^{(\dagger)}$ are the vibrational annihilation (creation) operators for a single mode of frequency ω_0. Coupling to the electronic degrees of freedom occurs via the dimensionless parameter Δ, which is related to the Huang-Rhys parameter, $S = \frac{1}{2}\Delta^2$, giving a reorganisation energy, $\hbar\lambda = \hbar S\omega_0$.[1]

The open quantum system incorporates baths that are constructed from an infinite number of harmonic oscillators coupled linearly to the coordinates of the system.[1,55] The coupling to bath, n, is defined by the spectral density, $J_n(\omega)$, which is related to the correlation function through,[47,55]

$$C_n(t) = \frac{1}{\pi}\int_0^\infty \mathrm{d}\omega J_n(\omega) \left(\coth\left(\frac{\beta\hbar\omega}{2}\right)\cos\omega t - i\sin\omega t\right) \tag{4}$$

Different photophysical processes are described by the interaction of the system with different baths. Here, we treat the dephasing that results from fluctuations of the transition energy, IVR and fluorescence with three independent baths. All baths are assumed to be Ohmic, such that every spectral density can be adequately approximated with the Debye

form for an overdamped Brownian oscillator,

$$J_n(\omega) = 2\eta_n \frac{\omega\gamma_n}{\omega^2 + \gamma_n^2} \tag{5}$$

where $\hbar\eta_n$ is the reorganisation energy of the bath and γ_n is a measure of the bath timescale.[1,56,57]

Solving the bath correlation function for the Debye spectral density produces a form which can be expressed as the sum of exponential terms, eq 6, with the coefficients, c_{nk}, and Matsubara frequencies, $\nu_{nk}; k = 0, 1, \ldots, M$, defined by eqs 7 to 10.[56–58] The inverse temperature, β, is the same for each bath.

$$C_n(t) = \sum_{k=0}^{M} c_{nk} e^{-\nu_{nk}|t|} \tag{6}$$

$$c_{n0} = \eta_n\gamma_n \left(\cot\left(\frac{\hbar\beta\gamma_n}{2}\right) - i \right) \tag{7}$$

$$c_{nk} = \frac{4\eta_n\gamma_n}{\hbar\beta} \left(\frac{\nu_{nk}}{\nu_{nk}^2 - \gamma_n^2} \right) \tag{8}$$

$$\nu_{n0} = \gamma_n \tag{9}$$

$$\nu_{nk} = \frac{2\pi k}{\hbar\beta} \tag{10}$$

As the vibrational mode included explicitly in the system Hamiltonian is of the same order as the fluctuations of the baths, non-Markovian dynamics must be employed to correctly account for memory effects, including the emergence of inhomogeneous distributions within the ensemble.[48,52,59,60] Therefore, in order to rigorously incorporate inhomogeneous broadening into the simulations, we employ the non-Markovian hierarchical equations of motion (HEOM) to evolve the density matrix. This involves propagating a number of auxiliary density operators (ADO), in addition to the true density matrix, to fully account for memory effects in the bath correlations.[56,61] The evolution of the density matrix is given by equation 11.[57]

$$\begin{aligned}\dot{\rho}_{\mathbf{j}}(t) &= -\left(\frac{i}{\hbar}\mathcal{L} + \sum_{n=1}^{N}\sum_{k=0}^{M}\mathbf{j}_{nk}\nu_{nk}\right)\rho_{\mathbf{j}}(t) - i\sum_{n=1}^{N}\sum_{k=0}^{M}B_n^{\times}\rho_{\mathbf{j}_{nk}^{+}}(t) \\ &\quad -i\sum_{n=1}^{N}\sum_{k=0}^{M}\mathbf{j}_{nk}\left(c_{nk}B_n\rho_{\mathbf{j}_{nk}^{-}}(t) - c_{nk}^{*}\rho_{\mathbf{j}_{nk}^{-}}(t)B_n\right) \\ &\quad -\sum_{n=1}^{N}\left(\frac{2\eta_n}{\hbar\beta\gamma_n} - \eta_n\cot\left(\frac{\hbar\beta\gamma_n}{2}\right) - \sum_{k=1}^{M}\frac{c_{nk}}{\nu_{nk}}\right)B_n^{\times}B_n^{\times}\rho_{\mathbf{j}}(t) \end{aligned} \tag{11}$$

Here, $B_n^{\times}\rho = [B_n, \rho]$ denotes the commutator of the bath coupling operator, B_n, with the density matrix. $\mathcal{L}$ is the Liouvillian operator, which explicitly incorporates the system-field interaction, $H_{SF}(t)$, via the semi-classical dipole approximation, where $\hat{\mu}$ is the dipole moment operator of the system and $\mathcal{E}(\mathbf{r}, t)$ the electric field of the incident laser.[50]

$$\mathcal{L}\rho(t) = [H_{\mathrm{S}} - H_{SF}(t), \rho(t)] = [H_{\mathrm{S}} - \hat{\mu}\cdot\mathcal{E}(\mathbf{r}, t), \rho(t)] \tag{12}$$

The ADOs are defined by the $N(M+1)$-dimensional vectors $\mathbf{j} = (j_{10}, \ldots, j_{nk}, \ldots, j_{NM})$ and $\mathbf{j}^{\pm} = (j_{10}, \ldots, j_{nk} \pm 1, \ldots, j_{NM})$, which contain an element for every Matsubara frequency associated with each contributing bath.[58,61] The individual elements, j_{nk}, define the hierarchical level of a particular Matsubara frequency.

The hierarchy is terminated via selection of a convergence parameter, Γ, which is significantly greater than the energy scales of the system-bath coupling; as described by Dijkstra and Prokhorenko.[57] Elements of the hierarchy which are deep enough to correspond to fluctuations faster than this convergence parameter are assumed to be Markovian. The termination criterion is expressed as

$$\sum_{n=1}^{N}\sum_{k=0}^{M}\mathbf{j}_{nk}\nu_{nk} > \Gamma \tag{13}$$

Photon echo spectroscopy involves the interaction of the system with the electric fields of three laser pulses. The first two pulses are separated by the coherence time, τ, and the second and third by the population time, T. The centre of the third pulse is defined to be

$t = 0$, with the third order polarization observed as a decaying oscillation for $t > 0$, emitted in the phase-matched direction, $\mathbf{k}_\mathrm{s}$.[62]

The macroscopic polarization resulting from the photon echo measurement in the rephasing ($\mathbf{k}_\mathrm{s} = -\mathbf{k}_1 + \mathbf{k}_2 + \mathbf{k}_3$) or non-rephasing ($\mathbf{k}_\mathrm{s} = \mathbf{k}_1 - \mathbf{k}_2 + \mathbf{k}_3$) direction is calculated using the equation of motion-phase matching approach (EOM-PMA), developed by Gelin et al.[45,46] The system-field interaction Hamiltonian is separated into the contributions of the three electric fields, $V_m(t)$: $m = 1, 2, 3$, according to,

$$\begin{aligned} \hat{H}_{SF}(t) &= -\sum_{m=1}^{3} \hat{\mu} \cdot (\chi_m E_m(t - \tau_m) \exp(-i\omega_m t + i\mathbf{k}_m \mathbf{r})) + c.c. \\ &= -\sum_{m=1}^{3} \exp(i\mathbf{k}_m \mathbf{r}) \cdot V_m(t) + c.c. \end{aligned} \tag{14}$$

where $\omega_m = 2\pi\nu_m$ has an associated wavevector, $\mathbf{k}_m$. The field envelope, centred at τ_m, is denoted $E(t - \tau_m)$ and is assumed to be Gaussian, with χ_m as a controllable factor for the intensity.[51,63] Differences in the temporal phase of the pulses, leading to pulse chirp, can be included by introducing an additional $\exp(+i\phi_m(t))$ factor in equation 14.[64,65] However, unchirped Gaussian pulses provide a suitable approximation for the laser spectra used by Camargo et al.

The third order polarization in the phase matched direction, $\mathbf{k}_s$, is then obtained by,

$$P^{(3)}_{\mathbf{k}_s}(\tau, T, t) = \exp(i\mathbf{k}_s \mathbf{r}) \mathbf{Tr} \left[\hat{\mu} \left(\rho_1(t) - \rho_2(t) - \rho_3(t) + \rho_4(t) - \rho_5(t) + \rho_6(t) + \rho_7(t)\right)\right] + c.c. \tag{15}$$

where $\rho_i(t); i = 0, 1, \ldots, 7$ are additional non-Hermitian auxiliary density operators, individually evolved using equation 11.[46] Each has a different Liouvillian operator that acts as a generating function for Liouville pathways, such that their combination in equation 15 removes the contribution of all except the pathways of interest in the phase matched direction.[45] Full details are provided in the SI. Two-dimensional photon echo spectra are then calculated as the double Fourier transform of the third order polarization with respect to τ

and t.[50,66]

Results and Discussion

The laser spectra and experimental linear absorption spectrum of the zinc porphyrin monomer are displayed in figure 1. In addition to the Q_x band, the experimental spectrum also shows a weaker absorption band at ca. $17\,000\,\mathrm{cm}^{-1}$. This corresponds to the Q_y band and any coupling to higher frequency vibrational modes, which are not considered here.[67]

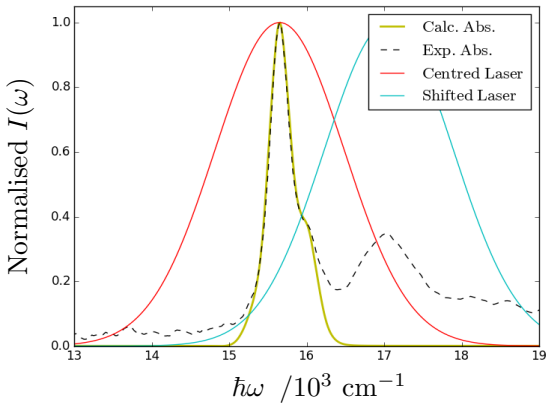

Figure 1: Calculated (gold) and experimental (dashed) linear absorption spectra for the zinc porphyrin monomer, with the centred (red) and blue-shifted (cyan) laser spectra.

The system parameters are $\omega_{eg}^0 = 15\,650\,\mathrm{cm}^{-1}$, with $\omega_0 = 375\,\mathrm{cm}^{-1}$ and $\Delta = 0.8$ such that $\lambda = 120\,\mathrm{cm}^{-1}$. Each electronic state is coupled to two vibrational levels. The simulations were performed at 300 K with the spectral density parameters for the dephasing bath set as $\eta_1 = 11\,\mathrm{cm}^{-1}$ and $\gamma_1 = 50\,\mathrm{cm}^{-1}$, for the IVR bath as $\eta_2 = 11\,\mathrm{cm}^{-1}$ and $\gamma_2 = 50\,\mathrm{cm}^{-1}$, and for the fluorescence bath as $\eta_3 = 1\,\mathrm{cm}^{-1}$ and $\gamma_3 = 50\,\mathrm{cm}^{-1}$. These parameters produced the calculated linear absorption spectrum in figure 1, which gives a good fit to the experimental spectrum.

Two simulations were performed, one with a laser spectrum centred at the fundamental transition of $\omega_m = 15\,650\,\mathrm{cm}^{-1}$ (figure 1, red), and another which was blue-shifted to $\omega_m = 17\,060\,\mathrm{cm}^{-1}$ (figure 1, cyan). Both laser spectra have a temporal FWHM of 15 fs for

the Gaussian envelopes. 2D photon echo spectra, presented as excitation axis, ω_τ, against emission axis, ω_t, were then calculated over 1 ps of population time, T. Figure 2 (left) shows an example rephasing photon echo spectrum for $T = 120$ fs from the centred laser spectrum simulation. The elongation of the main peak about the diagonal demonstrates inhomogeneous broadening, resulting from the dephasing bath ($n = 1$).

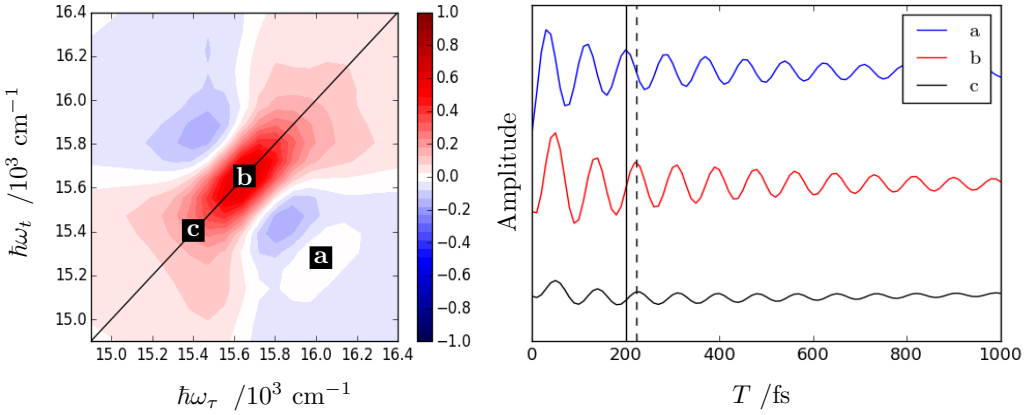

Figure 2: (Left) Normalised Real Rephasing 2D spectrum for $T = 120$ fs. (Right) Amplitude oscillations of the real rephasing component for the coordinates (a) (16025, 15275), (b) (15650, 15650) and (c) (15400, 15400), presented as (ω_τ, ω_t) in cm^{-1}, arbitrarily offset for clarity. The vertical lines in (right) demonstrate that (b) and (c) are 90° phase shifted with respect to (a).

Each peak in a 2D spectrum is the result of one or more unique Liouville pathways. In addition to rephasing and non-rephasing, these can be further classified as population or coherence pathways dependent on the state of the system during the population time. Population pathways correspond to non-oscillatory diagonal states and show an exponential decay with the population time due to relaxation, whilst coherence pathways, involving off-diagonal superpositions, oscillate at a frequency equal to the energy difference between states.[6,43] We further define positively oscillating coherences as e.g. $|g_0\rangle\langle g_1| \propto e^{+i\omega_0 T}$ and negatively oscillating coherences as e.g. $|g_1\rangle\langle g_0| \propto e^{-i\omega_0 T}$.

Figure 2 (right) shows the amplitude oscillations of three coordinates in the (ω_τ, ω_t) plane along the T axis. These oscillations were obtained after removal of the non-oscillatory exponential decay component corresponding to population pathways. The decay in the oscil-

lations is a result of coupling to the IVR bath ($n = 2$). In agreement with the experimental results of Camargo et al, there is a 90° phase shift in the oscillations between the diagonal, (b, c), and off-diagonal, (a), locations, with the oscillations of (c) being less intense than those of (a) and (b).[25] This supports the findings of Butkus et al, who theoretically examined the phase of the oscillation of a single coherence pathway and predicted that rephasing coherence pathways have a constant phase along their diagonal lineshape, but a varying phase along their anti-diagonal lineshape.[43,68]

Removing the non-oscillatory population pathways from all coordinates in the (ω_τ, ω_t) plane and performing a third Fourier transform over the population time, produces a series of amplitude spectra for positive and negative oscillatory components.[20] Peaks in the amplitude spectra at the mode frequency, $\omega_T = \pm\omega_0$, therefore correspond to coherence pathways of the coupled vibrational mode. An example negative rephasing coherence pathway is given in figure 3, labelled as R_2 using the 2D electronic spectroscopy convention. As this involves the lower transition frequency of $\omega_{eg}^0 - \omega_0$, blue-shifting the laser spectrum eliminates this pathway from the 2D spectra. On inspection of all the possible Liouville pathways, the locations of peaks in the rephasing and non-rephasing amplitude spectra are easily identified.[26,69]

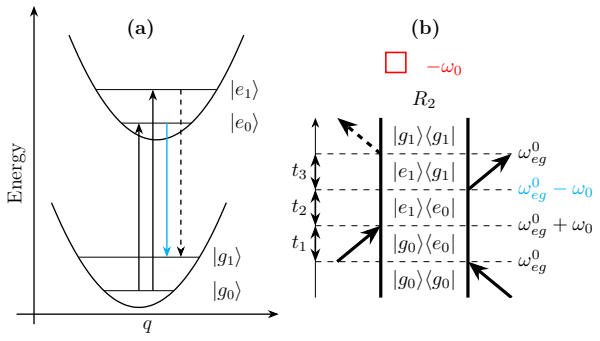

Figure 3: Example negative rephasing coherence pathway drawn onto the displaced harmonic oscillator potential energy surface in (a) and as a double-sided Feynman diagram in (b). The lower, hot band, transition frequency (highlighted in cyan) is not covered by the blue-shifted laser spectrum, identifying this as one of the eliminated pathways.

For the simulation with the centred laser spectrum, analysis of the coherence pathways predicts peaks in the rephasing and non-rephasing amplitude spectra as per diagrams (1a)

and (1b) of figure 4, respectively.[26] Six positive coherence pathways produce a square arrangement of four peaks below the diagonal for the positive rephasing amplitude spectrum, as shown by the calculated and experimental spectra, respectively (2c) and (3c) of figure 4. The two negative coherence pathways give two peaks aligned along $\omega_\tau = \omega_{eg}^0$, which are again visible in the calculated, (2a), and experimental, (3a), results in figure 4. Both the negative coherences correspond to stimulated emission pathways, whilst all four ground state bleach pathways appear in the positive spectrum. Similarly, the negative non-rephasing amplitude spectra show a square of four peaks in (2b) and (3b) of figure 4, with two peaks, again aligned along $\omega_\tau = \omega_{eg}^0$, in the equivalent positive amplitude spectra of (2d) and (3d), figure 4. In this case the four ground state bleach pathways appear in the positive spectrum, with the negative spectrum consisting of only stimulated emission pathways. All pathways are presented in the SI and all amplitude spectra are presented as an absolute value, normalised to their respective maxima. The experimental spectra are reproduced from reference 26.

On blue-shifting the laser spectrum, the majority of coherence pathways are eliminated, leaving a single ground state bleach and two stimulated emission pathways in each of the rephasing and non-rephasing amplitude spectra; as shown in diagrams (1a) and (1b) of figure 5. Each of the amplitude spectra feature a single peak, which is off-diagonal for the positive and negative rephasing spectra, respectively (2c)/(3c) and (2a)/(3a) of figure 5, and diagonal for the positive and negative non-rephasing spectra, respectively (2d)/(3d) and (2b)/(3b) of figure 5.

The elimination of coherence pathways is demonstrated by the change in position of the maximum intensity of the amplitude spectra. With a centred laser spectrum, this maximum appears between the predicted peak locations of (1a)/(1b) of figure 4, where the amplitude of adjacent peaks sums. This leads to the square arrangement in (2c)/(3c) and (2b)/(3b) of figure 4 and the elongated shape in (2a)/(3a) and (2d)/(3d) of figure 4. With a blue-shifted laser spectrum, the loss of adjacent peaks results in the maximum intensity exactly corresponding to the predicted peak locations, identified as the intersection of the dashed lines in

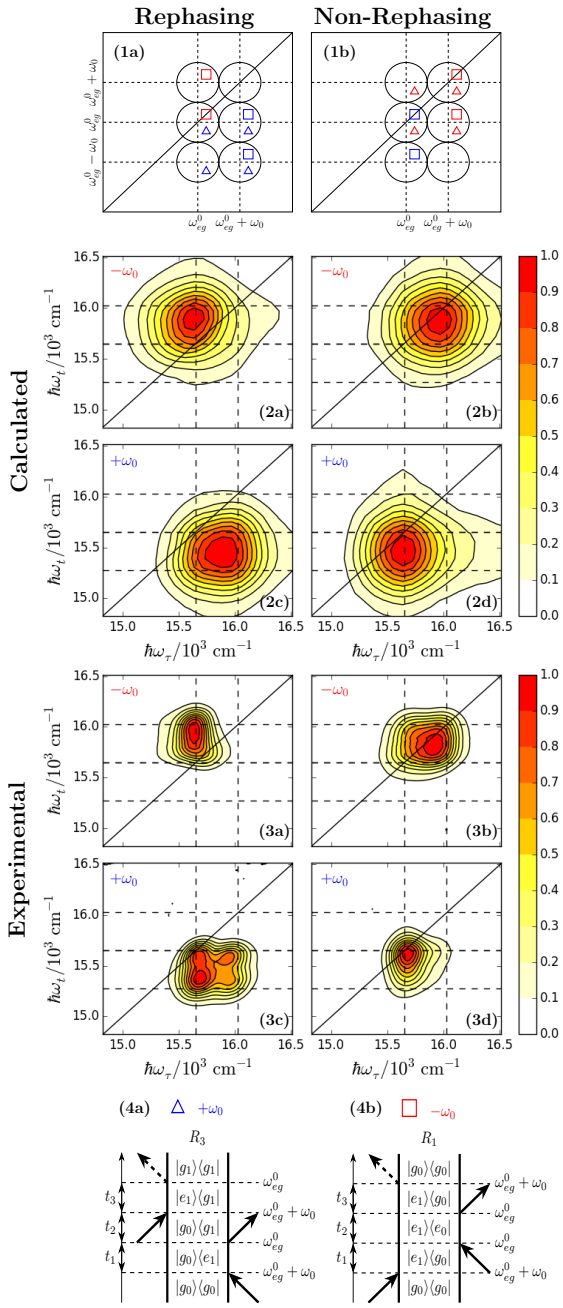

Figure 4: Predicted peak location key diagrams for rephasing (1a) and non-rephasing (1b) amplitude spectra, for the centred laser spectrum experiment. △/△ and □/□ correspond to positive/negative ground state bleach and stimulated emission coherence pathways, respectively, where the peaks are centred by their enclosing black circle. The calculated amplitude spectra are presented as the normalised absolute value, where (2a) and (2b) are respectively the rephasing and non-rephasing negative coherence maps, whilst (2c) and (2d) are the equivalent positive coherence maps. The experimental amplitude spectra are presented likewise as (3a-d), reproduced from reference 26. (4a) and (4b) are example double-sided Feynman diagrams for respectively positive ground state bleach rephasing and negative stimulated emission non-rephasing coherence pathways.

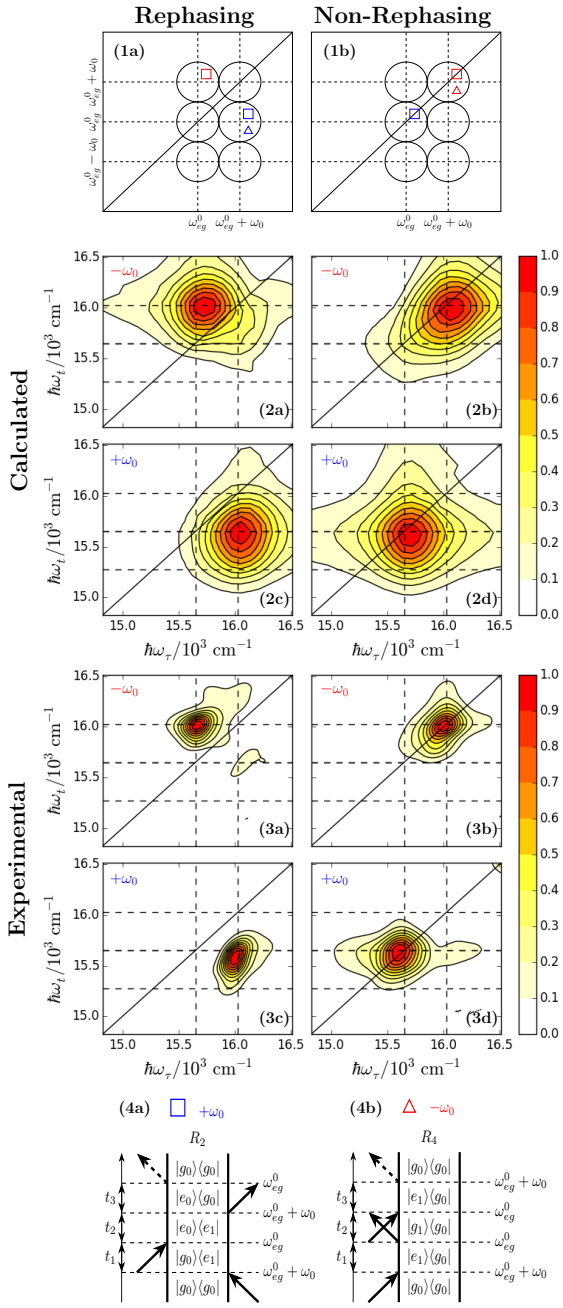

Figure 5: (1) - (3) are the same as in figure 4, for the experiment with the blue-shifted laser spectrum. (4a) and (4b) are example double-sided Feynman diagrams for respectively positive stimulated emission rephasing and negative ground state bleach non-rephasing coherence pathways.

figure 5. Any small offsets from the reported frequencies are a result of the discretization of data.

The additional broadening in the calculated amplitude spectra of both figures 4 and 5 is a result of the approximations within the model system. Namely, the bath parameters were selected based on the assumption that the $375\,\mathrm{cm}^{-1}$ mode is solely responsible for the lineshape of the Q_x band in the linear absorption spectrum. However, other vibrational modes neglected in this model would also contribute to the linear lineshape, but do not feature in the amplitude spectra specific to the $375\,\mathrm{cm}^{-1}$ mode. Hence the experimental amplitude spectra are less broad than their calculated equivalents. As it is the peak locations rather than the spectral broadening that is important for the Liouville pathway analysis, the model conclusively demonstrates the spectral filtering effects induced by blue-shifting the laser spectrum.

Conclusions

For both the centred and blue-shifted laser spectra simulations, the calculated amplitude spectra show excellent agreement with the experimental results and the predictions of the Liouville pathway analysis. The results presented in figures 4 and 5 clearly demonstrate the capability of the non-impulsive and non-Markovian model for the study of vibronic coherences isolated by a tunable laser spectrum. We have brought together a detailed vibronic Hamiltonian, a rigorous definition of the evolution of the bath and a method for calculating the non-linear polarization which explicitly incorporates the laser fields, to create a theoretical model suitable for studies involving spectral filtering effects.

For complex systems with broad absorption bands, spectral filtering can be exploited to focus 2D spectroscopic studies on specific regions.[36,44,70,71] But as shown in this work, spectral filtering can also be employed to control the pathways involved in a non-linear measurement and predictably eliminate certain pathways. Introducing the use of multicoloured laser pulses

also provides the potential for isolation of specific Liouville pathways.[28,72,73] This enables the study of particular coherences which, with the support of rigorous theoretical models such as that presented here, will lead to a greater understanding of the electronic and vibrational fine structure responsible for these spectral features.

Acknowledgement

The research presented in this paper was carried out on the High Performance Computing Cluster supported by the Research and Specialist Computing Support service at the University of East Anglia. F. V. A. C. thanks Brazilian Funding Agency Coordination for the Improvement of Higher Level Personnel (CAPES) for his doctoral studentship (BEX 9527/13-3). D. G. thanks the Faculty of Science at the University of East Anglia for his studentship funding.

Supporting Information Available

Supporting Information Available: Complete details of the model and Liouville pathway analysis, and additional examples of the calculated 2D spectra. This information is available free of charge via the Internet at http://pubs.acs.org

References

(1) Mukamel, S. *Principles of Nonlinear Optical Spectroscopy*; Oxford University Press: New York, 1995.

(2) Jonas, D. M. Two-Dimensional Femtosecond Spectroscopy. *Annu. Rev. Phys. Chem.* **2003**, *54*, 425–463.

(3) Petti, M. K.; Lomont, J. P.; Maj, M.; Zanni, M. T. Two-Dimensional Spectroscopy Is

Being Used to Address Core Scientific Questions in Biology and Materials Science. *J. Phys. Chem. B* **2018**, *122*, 1771–1780.

(4) Turner, D. B.; Wilk, K. E.; Curmi, P. M. G.; Scholes, G. D. Comparison of Electronic and Vibrational Coherence Measured by Two-Dimensional Electronic Spectroscopy. *J. Phys. Chem. Lett.* **2011**, *2*, 1904–1911.

(5) Scholes, G. D.; Fleming, G. R.; Chen, L. X.; Aspuru-Guzik, A.; Buchleitner, A.; Coker, D. F.; Engel, G. S.; van Grondelle, R.; Ishizaki, A.; Jonas, D. M. et al. Using Coherence to Enhance Function in Chemical and Biophysical Systems. *Nature* **2017**, *543*, 647–656.

(6) Dean, J. C.; Scholes, G. D. Coherence Spectroscopy in the Condensed Phase: Insights into Molecular Structure, Environment, and Interactions. *Acc. Chem. Res.* **2017**, *50*, 2746–2755.

(7) Brixner, T.; Stenger, J.; Vaswani, H. M.; Cho, M.; Blankenship, R. E.; Fleming, G. R. Two-Dimensional Spectroscopy of Electronic Couplings in Photosynthesis. *Nature* **2005**, *434*, 625–628.

(8) Engel, G. S.; Calhoun, T. R.; Read, E. L.; Ahn, T.-K.; Mančal, T.; Cheng, Y.-C.; Blankenship, R. E.; Fleming, G. R. Evidence for Wavelike Energy Transfer through Quantum Coherence in Photosynthetic Systems. *Nature* **2007**, *446*, 782–786.

(9) Schlau-Cohen, G. S.; Calhoun, T. R.; Ginsberg, N. S.; Read, E. L.; Ballottari, M.; Bassi, R.; van Grondelle, R.; Fleming, G. R. Pathways of Energy Flow in LHCII from Two-Dimensional Electronic Spectroscopy. *J. Phys. Chem. B* **2009**, *113*, 15352–15363.

(10) Collini, E.; Wong, C. Y.; Wilk, K. E.; Curmi, P. M. G.; Brumer, P.; Scholes, G. D. Coherently Wired Light-Harvesting in Photosynthetic Marine Algae at Ambient Temperature. *Nature* **2010**, *463*, 644–647.

(11) Panitchayangkoon, G.; Hayes, D.; Fransted, K. A.; Caram, J. R.; Harel, E.; Wen, J.; Blankenship, R. E.; Engel, G. S. Long-Lived Quantum Coherence in Photosynthetic Complexes at Physiological Temperature. *Proc. Natl. Acad. Sci. U. S. A.* **2010**, *107*, 12766–12770.

(12) Fassioli, F.; Dinshaw, R.; Arpin, P. C.; Scholes, G. D. Photosynthetic Light Harvesting: Excitons and Coherence. *J. R. Soc., Interface* **2013**, *11*, 20130901.

(13) Richards, G. H.; Wilk, K. E.; Curmi, P. M. G.; Davis, J. A. Disentangling Electronic and Vibrational Coherence in the Phycocyanin-645 Light-Harvesting Complex. *J. Phys. Chem. Lett.* **2014**, *5*, 43–49.

(14) Chenu, A.; Scholes, G. D. Coherence in Energy Transfer and Photosynthesis. *Annu. Rev. Phys. Chem.* **2015**, *66*, 69–96.

(15) Dostál, J.; Pšenčík, J.; Zigmantas, D. In Situ Mapping of the Energy Flow through the Entire Photosynthetic Apparatus. *Nat. Chem.* **2016**, *8*, 705–710.

(16) Dahlberg, P. D.; Ting, P.-C.; Massey, S. C.; Allodi, M. A.; Martin, E. C.; Hunter, C. N.; Engel, G. S. Mapping the Ultrafast Flow of Harvested Solar Energy in Living Photosynthetic Cells. *Nat. Commun.* **2017**, *8*, 988.

(17) Rolczynski, B. S.; Zheng, H.; Singh, V. P.; Navotnaya, P.; Ginzburg, A. R.; Caram, J. R.; Ashraf, K.; Gardiner, A. T.; Yeh, S.-h.; Kais, S. et al. Correlated Protein Environments Drive Quantum Coherence Lifetimes in Photosynthetic Pigment-Protein Complexes. *Chem* **2018**, *4*, 138–149.

(18) Harel, E.; Rupich, S. M.; Schaller, R. D.; Talapin, D. V.; Engel, G. S. Measurement of Electronic Splitting in PbS Quantum Dots by Two-Dimensional Nonlinear Spectroscopy. *Phys. Rev. B* **2012**, *86*, 075412.

(19) Fingerhut, B. P.; Richter, M.; Luo, J.-W.; Zunger, A.; Mukamel, S. 2D Optical Photon Echo Spectroscopy of a Self-Assembled Quantum Dot. *Ann. Phys. (Berlin, Ger.)* **2013**, *525*, 31–42.

(20) Seibt, J.; Pullerits, T. Beating Signals in 2D Spectroscopy: Electronic or Nuclear Coherences? Application to a Quantum Dot Model System. *J. Phys. Chem. C* **2013**, *117*, 18728–18737.

(21) Tollerud, J. O.; Cundiff, S. T.; Davis, J. A. Revealing and Characterizing Dark Excitons through Coherent Multidimensional Spectroscopy. *Phys. Rev. Lett.* **2016**, *117*, 097401.

(22) Mančal, T.; Christensson, N.; Lukeš, V.; Milota, F.; Bixner, O.; Kauffmann, H. F.; Hauer, J. System-Dependent Signatures of Electronic and Vibrational Coherences in Electronic Two-Dimensional Spectra. *J. Phys. Chem. Lett.* **2012**, *3*, 1497–1502.

(23) Duan, H.-G.; Nalbach, P.; Prokhorenko, V. I.; Mukamel, S.; Thorwart, M. On the Origin of Oscillations in Two-Dimensional Spectra of Excitonically-Coupled Molecular Systems. *New J. Phys.* **2015**, *17*, 072002.

(24) Tempelaar, R.; Halpin, A.; Johnson, P. J. M.; Cai, J.; Murphy, R. S.; Knoester, J.; Miller, R. J. D.; Jansen, T. L. C. Laser-Limited Signatures of Quantum Coherence. *J. Phys. Chem. A* **2016**, *120*, 3042–3048.

(25) Camargo, F. V. A.; Anderson, H. L.; Meech, S. R.; Heisler, I. A. Full Characterization of Vibrational Coherence in a Porphyrin Chromophore by Two-Dimensional Electronic Spectroscopy. *J. Phys. Chem. A* **2015**, *119*, 95–101.

(26) Camargo, F. V. A.; Grimmelsmann, L.; Anderson, H. L.; Meech, S. R.; Heisler, I. A. Resolving Vibrational from Electronic Coherences in Two-Dimensional Electronic Spectroscopy: The Role of the Laser Spectrum. *Phys. Rev. Lett.* **2017**, *118*, 033001.

(27) Moca, R.; Meech, S. R.; Heisler, I. A. Two-Dimensional Electronic Spectroscopy of Chlorophyll a: Solvent Dependent Spectral Evolution. *J. Phys. Chem. B* **2015**, *119*, 8623–8630.

(28) Senlik, S. S.; Policht, V. R.; Ogilvie, J. P. Two-Color Nonlinear Spectroscopy for the Rapid Acquisition of Coherent Dynamics. *J. Phys. Chem. Lett.* **2015**, *6*, 2413–2420.

(29) Meneghin, E.; Leonardo, C.; Volpato, A.; Bolzonello, L.; Collini, E. Mechanistic Insight into Internal Conversion Process Within Q-Bands of Chlorophyll a. *Sci. Rep.* **2017**, *7*, 11389.

(30) Ginsberg, N. S.; Cheng, Y.-C.; Fleming, G. R. Two-Dimensional Electronic Spectroscopy of Molecular Aggregates. *Acc. Chem. Res.* **2009**, *42*, 1352–1363.

(31) Halpin, A.; Johnson, P. J. M.; Tempelaar, R.; Murphy, R. S.; Knoester, J.; Jansen, T. L. C.; Miller, R. J. D. Two-Dimensional Spectroscopy of a Molecular Dimer Unveils the Effects of Vibronic Coupling on Exciton Coherences. *Nat. Chem.* **2014**, *6*, 196–201.

(32) Camargo, F. V. A.; Anderson, H. L.; Meech, S. R.; Heisler, I. A. Time-Resolved Twisting Dynamics in a Porphyrin Dimer Characterized by Two-Dimensional Electronic Spectroscopy. *J. Phys. Chem. B* **2015**, *119*, 14660–14667.

(33) Lim, J.; Paleček, D.; Caycedo-Soler, F.; Lincoln, C. N.; Prior, J.; von Berlepsch, H.; Huelga, S. F.; Plenio, M. B.; Zigmantas, D.; Hauer, J. Vibronic Origin of Long-Lived Coherence in an Artificial Molecular Light Harvester. *Nat. Commun.* **2015**, *6*, 7755.

(34) Bolzonello, L.; Fassioli, F.; Collini, E. Correlated Fluctuations and Intraband Dynamics of J-Aggregates Revealed by Combination of 2DES Schemes. *J. Phys. Chem. Lett.* **2016**, *7*, 4996–5001.

(35) Wang, L.; Griffin, G. B.; Zhang, A.; Zhai, F.; Williams, N. E.; Jordan, R. F.; Engel, G. S.

Controlling Quantum-Beating Signals in 2D Electronic Spectra by Packing Synthetic Heterodimers on Single-Walled Carbon Nanotubes. *Nat. Chem.* **2017**, *9*, 219–225.

(36) Cipolloni, M.; Fresch, B.; Occhiuto, I.; Rukin, P.; Komarova, K. G.; Cecconello, A.; Willner, I.; Levine, R. D.; Remacle, F.; Collini, E. Coherent Electronic and Nuclear Dynamics in a Rhodamine Heterodimer-DNA Supramolecular Complex. *Phys. Chem. Chem. Phys.* **2017**, *19*, 23043–23051.

(37) Kullmann, M.; Ruetzel, S.; Buback, J.; Nuernberger, P.; Brixner, T. Reaction Dynamics of a Molecular Switch Unveiled by Coherent Two-Dimensional Electronic Spectroscopy. *J. Am. Chem. Soc.* **2011**, *133*, 13074–13080.

(38) Anna, J. M.; Baiz, C. R.; Ross, M. R.; Mccanne, R.; Kubarych, K. J. Ultrafast Equilibrium and Non-Equilibrium Chemical Reaction Dynamics Probed with Multidimensional Infrared Spectroscopy. *Int. Rev. Phys. Chem.* **2012**, *31*, 367–419.

(39) Ruetzel, S.; Diekmann, M.; Nuernberger, P.; Walter, C.; Engels, B.; Brixner, T. Multidimensional Spectroscopy of Photoreactivity. *Proc. Natl. Acad. Sci. U. S. A.* **2014**, *111*, 4764–4769.

(40) Kiefer, L. M.; King, J. T.; Kubarych, K. J. Dynamics of Rhenium Photocatalysts Revealed through Ultrafast Multidimensional Spectroscopy. *Acc. Chem. Res.* **2015**, *48*, 1123–1130.

(41) Nuernberger, P.; Ruetzel, S.; Brixner, T. Multidimensional Electronic Spectroscopy of Photochemical Reactions. *Angew. Chem., Int. Ed.* **2015**, *54*, 11368–11386.

(42) Bolzonello, L.; Polo, A.; Volpato, A.; Meneghin, E.; Cordaro, M.; Trapani, M.; Fortino, M.; Pedone, A.; Castriciano, M. A.; Collini, E. Two-Dimensional Electronic Spectroscopy Reveals Dynamics and Mechanisms of Solvent-Driven Inertial Relaxation in Polar BODIPY Dyes. *J. Phys. Chem. Lett.* **2018**, *9*, 1079–1085.

(43) Butkus, V.; Zigmantas, D.; Valkunas, L.; Abramavicius, D. Vibrational vs. Electronic Coherences in 2D Spectrum of Molecular Systems. *Chem. Phys. Lett.* **2012**, *545*, 40–43.

(44) Maiuri, M.; Ostroumov, E. E.; Saer, R. G.; Blankenship, R. E.; Scholes, G. D. Coherent Wavepackets in the Fenna-Matthews-Olson Complex are Robust to Excitonic-Structure Perturbations caused by Mutagenesis. *Nat. Chem.* **2018**, *10*, 177–183.

(45) Gelin, M. F.; Egorova, D.; Domcke, W. Efficient Method for the Calculation of Time- and Frequency-Resolved Four-Wave Mixing Signals and its Application to Photon-Echo Spectroscopy. *J. Chem. Phys.* **2005**, *123*, 164112.

(46) Gelin, M. F.; Egorova, D.; Domcke, W. Efficient Calculation of Time- and Frequency-Resolved Four-Wave-Mixing Signals. *Acc. Chem. Res.* **2009**, *42*, 1290–1298.

(47) Tanimura, Y. Nonperturbative Expansion Method for a Quantum System Coupled to a Harmonic-Oscillator Bath. *Phys. Rev. A* **1990**, *41*, 6676–6687.

(48) Tanimura, Y. Stochastic Liouville, Langevin, Fokker-Planck, and Master Equation Approaches to Quantum Dissipative Systems. *J. Phys. Soc. Jpn.* **2006**, *75*, 082001.

(49) de Vega, I.; Alonso, D. Dynamics of Non-Markovian Open Quantum Systems. *Rev. Mod. Phys.* **2017**, *89*, 015001.

(50) Leng, X.; Yue, S.; Weng, Y.-X.; Song, K.; Shi, Q. Effects of Finite Laser Pulse Width on Two-Dimensional Electronic Spectroscopy. *Chem. Phys. Lett.* **2017**, *667*, 79–86.

(51) Sharp, L. Z.; Egorova, D.; Domcke, W. Efficient and Accurate Simulations of Two-Dimensional Electronic Photon-Echo Signals: Illustration for a Simple Model of the Fenna-Matthews-Olson Complex. *J. Chem. Phys.* **2010**, *132*, 014501.

(52) Tanimura, Y. Real-Time and Imaginary-Time Quantum Hierarchal Fokker-Planck Equations. *J. Chem. Phys.* **2015**, *142*, 144110.

(53) Sala, M.; Egorova, D. Two-Dimensional Photon-Echo Spectroscopy at a Conical Intersection: A Two-Mode Pyrazine Model with Dissipation. *Chem. Phys.* **2016**, *481*, 206–217.

(54) Egorova, D.; Gelin, M. F.; Domcke, W. Analysis of Cross Peaks in Two-Dimensional Electronic Photon-Echo Spectroscopy for Simple Models with Vibrations and Dissipation. *J. Chem. Phys.* **2007**, *126*, 074314.

(55) Dijkstra, A. G.; Tanimura, Y. Linear and Third- and Fifth-Order Nonlinear Spectroscopies of a Charge Transfer System Coupled to an Underdamped Vibration. *J. Chem. Phys.* **2015**, *142*, 212423.

(56) Dijkstra, A. G.; Tanimura, Y. System Bath Correlations and the Nonlinear Response of Qubits. *J. Phys. Soc. Jpn.* **2012**, *81*, 063301.

(57) Dijkstra, A. G.; Prokhorenko, V. I. Simulation of Photo-Excited Adenine in Water with a Hierarchy of Equations of Motion Approach. *J. Chem. Phys.* **2017**, *147*, 064102.

(58) Chen, L.; Zheng, R.; Shi, Q.; Yan, Y. Optical Line Shapes of Molecular Aggregates: Hierarchical Equations of Motion Method. *J. Chem. Phys.* **2009**, *131*, 094502.

(59) Tanimura, Y.; Ishizaki, A. Modeling, Calculating, and Analyzing Multidimensional Vibrational Spectroscopies. *Acc. Chem. Res.* **2009**, *42*, 1270–1279.

(60) Tanimura, Y. Reduced Hierarchy Equations of Motion Approach with Drude plus Brownian Spectral Distribution: Probing Electron Transfer Processes by means of Two-Dimensional Correlation Spectroscopy. *J. Chem. Phys.* **2012**, *137*, 22A550.

(61) Ishizaki, A.; Tanimura, Y. Nonperturbative Non-Markovian Quantum Master Equation: Validity and Limitation to Calculate Nonlinear Response Functions. *Chem. Phys.* **2008**, *347*, 185–193.

(62) Brixner, T.; Mančal, T.; Stiopkin, I. V.; Fleming, G. R. Phase-Stabilized Two-Dimensional Electronic Spectroscopy. *J. Chem. Phys.* **2004**, *121*, 4221–4236.

(63) Egorova, D. Oscillations in Two-Dimensional Photon-Echo Signals of Excitonic and Vibronic Systems: Stick-Spectrum Analysis and its Computational Verification. *J. Chem. Phys.* **2014**, *140*, 034314.

(64) Tekavec, P. F.; Myers, J. A.; Lewis, K. L. M.; Fuller, F. D.; Ogilvie, J. P. Effects of Chirp on Two-Dimensional Fourier Transform Electronic Spectra. *Opt. Express* **2010**, *18*, 11015.

(65) Christensson, N.; Avlasevich, Y.; Yartsev, A.; Müllen, K.; Pascher, T.; Pullerits, T. Weakly Chirped Pulses in Frequency Resolved Coherent Spectroscopy. *J. Chem. Phys.* **2010**, *132*, 174508.

(66) Cheng, Y.-C.; Engel, G. S.; Fleming, G. R. Elucidation of Population and Coherence Dynamics using Cross-Peaks in Two-Dimensional Electronic Spectroscopy. *Chem. Phys.* **2007**, *341*, 285–295.

(67) Drobizhev, M.; Stepanenko, Y.; Dzenis, Y.; Karotki, A.; Rebane, A.; Taylor, P. N.; Anderson, H. L. Extremely Strong Near-IR Two-Photon Absorption in Conjugated Porphyrin Dimers: Quantitative Description with Three-Essential-States Model. *J. Phys. Chem. B* **2005**, *109*, 7223–7236.

(68) Butkus, V.; Zigmantas, D.; Abramavicius, D.; Valkunas, L. Distinctive Character of Electronic and Vibrational Coherences in Disordered Molecular Aggregates. *Chem. Phys. Lett.* **2013**, *587*, 93–98.

(69) Caram, J. R.; Fidler, A. F.; Engel, G. S. Excited and Ground State Vibrational Dynamics Revealed by Two-Dimensional Electronic Spectroscopy. *J. Chem. Phys.* **2012**, *137*, 024507.

(70) Wells, K. L.; Lambrev, P. H.; Zhang, Z.; Garab, G.; Tan, H.-S. Pathways of Energy Transfer in LHCII Revealed by Room-Temperature 2D Electronic Spectroscopy. *Phys. Chem. Chem. Phys.* **2014**, *16*, 11640–11646.

(71) Dean, J. C.; Mirkovic, T.; Toa, Z. S.; Oblinsky, D. G.; Scholes, G. D. Vibronic Enhancement of Algae Light Harvesting. *Chem* **2016**, *1*, 858–872.

(72) Tollerud, J. O.; Hall, C. R.; Davis, J. A. Isolating Quantum Coherence using Coherent Multi-Dimensional Spectroscopy with Spectrally Shaped Pulses. *Opt. Express* **2014**, *22*, 6719.

(73) Novelli, F.; Nazir, A.; Richards, G. H.; Roozbeh, A.; Wilk, K. E.; Curmi, P. M. G.; Davis, J. A. Vibronic Resonances Facilitate Excited-State Coherence in Light-Harvesting Proteins at Room Temperature. *J. Phys. Chem. Lett.* **2015**, *6*, 4573–4580.

Graphical TOC Entry